Mining Science, vol. 30, 2023, 183–208

www.miningscience.pwr.edu.pl

Mining Science

(Previously Prace Naukowe Instytutu Gornictwa Politechniki Wroclawskiej, ISSN 0370-0798)

ISSN 2300-9586 (print)
ISSN 2353-5423 (online)

Received march 19, 2023; Reviewed; Accepted September 27, 2023

NEW APPROACH FOR THE ORES ADD-VALUE. CASE STUDY: THE PHYSICAL BENEFICIATION OF WHITE SAND IN EL-HARRA AREA, BAHARIYA OASIS, WESTERN DESERT, EGYPT

Mona M. FAWZY*, Reda A. EL-ARAFY, Ahmed E. ABDEL GAWAD, Mohammed A. EL-ZALAKY, Abdallah S. ALSHAMY, Ahmed Mousad ISMAIL, Marwa M. ABDEL-AZEEM, Rania ROSHDI, Sameh, H. NEGM, T. NASR, Hamid E. MIRA, Tarek F. MOHAMMADEN

Nuclear Materials Authority, P.O. Box 530 El-Maadi, Cairo, Egypt

Abstract: Integration of the remote sensing techniques including the thermal emission and reflection radiometer (ASTER) thermal infrared (TIR) data, and the silica index (SI) algorithms have enabled the discovery of a previously unknown white sand deposit in the El-Harra region of the Bahariya Oasis. The physical, chemical, and mineralogical characterization of El-Harra white sand was achieved using the binocular microscope, X-Ray Diffraction (XRD), X-Ray Fluorescence spectrometry (XRF) and Scanning Electron Microscopy (SEM). The sample was physically beneficiated using attrition scrubbing, shacking table concentration and magnetic separation while its heavy mineral content was conducted via heavy liquid separation. The chemical and grain size analysis before and after the physical treatment pointed to clear enhancing in both the chemical and grain size specifications, where the oxide ratios of SiO_2, Al_2O_3, Fe_2O_3 and CaO moved from 96.87, 0.82, 0.13 and 1.27% to 99.53, 0.05, 0.05 and 0.13%, respectively. On the other hand, the ratio of grain size (–0.5/+0.125 mm) was raised from 79.48% to 82.04% from the total sample weight. Comparing these data with their corresponding in both the British and American Standard Specifications of White Sand confirmed the validity of the physical beneficiation in raising the grade of the investigated white sand from low valuable ore to the globally highest one which means higher marketing prices and the availability to use the treated white sand in a wide spectrum of technological and strategic applications. Furthermore, the heavy minerals content and species is another add value, where their content was assigned as 0.3 mass% from the head sample including ilmenite, rutile, zircon,

* Corresponding author: mm1_fawzy@yahoo.com (Mona M. Fawzy)

doi: 10.37190/msc233013

leucoxene and green silicates. This simply means each 1000 tons of physically beneficiated white sand yield 3 tons of the heavy minerals.

***Keywords*:** *add value, physical beneficiation, silica index, White Sand, El-Harra, Bahariya Oasis*

1. INTRODUCTION

The white sand is the most famous name for certain sand deposits characterized by their white color. Other names are also used such as silica sand or quartz sand, these nomenclatures back to their strongly dominant SiO_2 as chemical composition and quartz as mineral component. However, different white sand grades can be recognized based on the ratios of SiO_2, Al_2O_3, Fe_2O_3 and CaO + MgO from the chemical composition point of view (British Standard (BS) 2975 1988 and Norton 1957).

In general, the white sand is considered as a main natural resource for wide spectrum of industries and application such as; glassmaking, metal casting, metal production, ceramic fabrication, painting, coating, filtration, water treatment, oil- and gas-wells drilling or even some of high-tech applications as optics, metal silicon, silicon weavers as well as some electronic and military devices (Nigussie et al. 2023). Therefore, many countries make respectful efforts to develop their resources from the white sand via different exploration programs and techniques. Traditional approaches for discovering and mapping these deposits, on the other hand, are frequently costly, time-consuming, and constrained by accessibility and environmental constraints. Remote sensing techniques, based on spectral signatures, provide an alternate method for identifying and characterizing white sand deposits (Rockwell and Hofstra 2008; Ali and Ghoneim 2022; Ninomiya et al. 2005).

The purity-grade of the white sand is the main factor controls its using in any of these applications. Accordingly, purification of the white sand ore is considered a vital issue for maximizing the economic benefits of this natural ore. In particular, the metal silicon production (and its subsequent products) requires high-purity silica sand up to 99.99% SiO_2, and reaching this percentage requires utilizing many physical and chemical methods in order to raise the grade of the raw material and get rid of the associated impurities (Boussaa et al. 2018).

The impurities in the silica sand are usually present as free and/or coated iron oxides, clay, titania and smaller amounts of sodium, potassium and calcium minerals. The iron, as the most detrimental impurity, and other impurities can be minimized by various physical, physico-chemical or chemical methods; however the proper method depends on the mineralogical forms and distribution of iron in the ore (Popa et al. 2022). The physical operations include; size separation (screening), gravity separation (spiral concentration), magnetic separation, etc., on the other hand, the physico-chemical (flotation) or even chemical methods (leaching) have to be occasionally adopted for effective removal of iron which may be in intimate association with the

mineral quite often superficially (Bhattacharya and Das, 1994; Taxiarchaou et al. 1997; Ay and Arica 2000, Farmer et al. 2000, wills 2016).

In the same regard, the present study concerns a recently discovered white sand deposit located in the El-Harra region of Bahariya Oasis, Egypt. The identification of this new occurrence was accomplished through the utilization of the silica index (SI) derived from Advanced Spaceborne Thermal Emission and Reflection Radiometer (ASTER) thermal infrared (TIR) data. Subsequently, a representative technological sample from this deposit was subjected to the laboratory investigation to define its grain-size, chemical, and mineralogical characteristics. In addition, the physical upgrading studies were applied to adopt simple, cost-effective and environmentally ecofriend beneficiation techniques for purifying the silica sand and evaluate their suitability for using in different advanced industrial applications, and hence creating add value for this newly discovered white sand deposit.

2. MATERIALS AND METHODS

2.1. SITE DESCRIPTION AND GEOLOGICAL BACKGROUND

The Bahariya Oasis is one of the most important geological provinces that provide insights into the paleontological, hydrogeological, and sedimentological history of the Western Desert, Egypt Its sedimentary cover include a thick sequence of marine, continental, and lacustrine deposits from the Mesozoic period. It contains economic and valuable ores, comprising phosphates, iron, barite, radioactive mineralization as well as hydrocarbon resources (Morsy 1987; El-Agami et al. 2005; El-Sharkawi et al. 2006; Abouelresh et al. 2007; El-Araby et al. 2007; Haroun and Raslan 2010; Ahmed 2011; Afify et al. 2015; El-Zalaky et al. 2018).

Bahariya Formation of the Cenomanian age is the most extensive and is composed of a diverse set of sedimentary succession and unconformably overlain by Eocene succession including dolostone, marl and limestones of Naqb, Qazzun and El Hamra formations. This sequence is truncated by Oligocene Radwan Formation represented by fluvial sandstone (El Akkad and Issawi 1963; Said and Issawi 1964; Hassan 2004; Ibrahim et al. 2014; Afify et al. 2015; Sallam et al. 2018; Sallam et al. 2020). The lithostratigraphic section of the Bahariya Formation is of about 75 m in thickness and composed of three members; the lower (composed of multi-layered package of siltstones, white sand, ironstone, sandstone and variegated carbonaceous and black shale), the middle (consists of laminated siltstone interbedd with massive sandstone and barite veins) and the upper (contains highly altered variegated shale, cross-bedded and massive sandstone, siltstone, ironstone and dolostone) (Fig. 1).

El-Harra area, where the new white sand deposit was discovered, locates to the northern of Bahariya Depression, Western Desert, Egypt (Fig. 2) and the white sand bed

occupies the lower sequence of Bahariya Formation reaching 5 m-thick in average. This deposit is generally characterized by its brightness, snow-white appearance, transparent, subround to rounded, fine- to coarse-size grains and almost composed of pure quartz (Fig. 3).

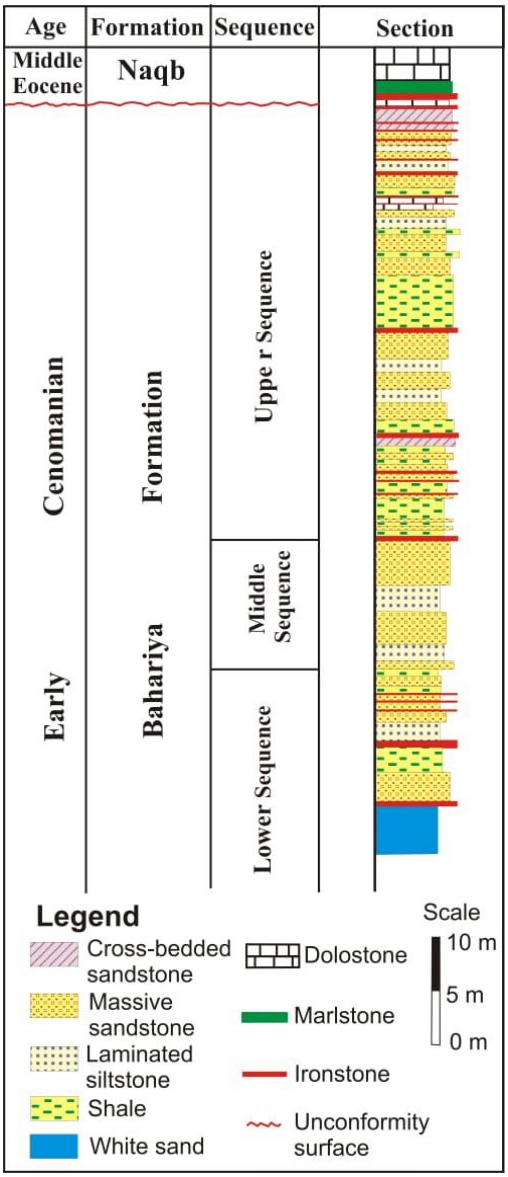

Fig. 1. The lithostratigraphic sections of El-Harra area, northern part of Bahariya Depression modified after (Said and Issawi 1964, Afify et al. 2015)

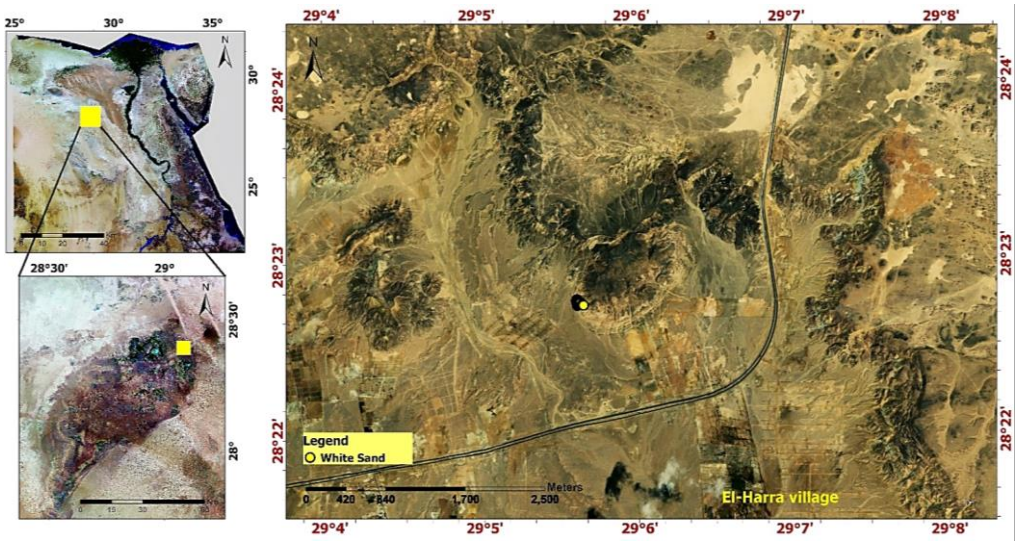

Fig. 2. Location map showing El-Harra area to the northern part
of Bahariya Depression

Fig. 3. The white sand deposit in El-Harra area, Bahariya Depression,
Western Desert, Egypt

2.2. REMOTE SENSING DATA AND TECHNIQUES

The Advanced Spaceborne Thermal Emission and Reflection Radiometer (ASTER) sensor onboard the Earth Observing System (EOS) Terra satellite, which was launched in 2000, offers ground-breaking new capabilities for cost-effective mineral and landcover imaging across wide regions. The ASTER Level 1B radiance data were used to calculate the surface emissivity using the temperature-emissivity separation (TES) algorithm and then applied the silica indices (SI) technique. The Level 1B data were processed from the original Level 1A format by the Earth Remote Sensing Data Analysis Center (ERSDAC) of Japan. A cloud-free scene of ASTER emissivity data was acquired 29 May 2001 and obtained from EROS and re-sampled to the geographic projection using a nearest-neighborkernal based on satellite ephemeris data contained within the data files.

2.3. PHYSICAL BENEFICIATION METHODOLOGY

Ten trenches (3 meters in depth) were executed throughout the studied area, and several samples were collected (one sample per each meter), and then all the samples were added together in one representative head sample (weighting about 50 kg). Initially and after well blending, the head sample was split into representative fractions using John's riffle Splitter in order to be ready for various characterization, tests and beneficiation processes. While one fraction was kept as a reference sample, the other fractions were subjected to the following studies:

Granulometric analyses: to determine the grains size range and the relative weight percentages of each size. This experiment was carried out using the mechanical sieve shaker with a set of sieves have aperture diameters of 2.0, 1.0, 0.5, 0.250, 0.125, and 0.063 mm (ASTM codes);

Gravimetric investigation: to measure the moisture content by drying the white sand fractions at 105 °C and weighing them before and after the dryness process;

The chemical analysis: to identify and quantify both the major and trace components in the original sample, the obtained fractionated sizes and the final products after beneficiation. All the samples were firstly ground to less than 75 μm by the agate mortar, and then subjected the chemical analyses using the X-ray fluorescence (XRF) spectrometry (Axios advanced, Sequential WD_XRF Spectrometer) with detection limit at 20 and 2 ppm for the major and trace elements, respectively;

Mineralogical identification: was carried out for the individual minerals which handily picked under Olympus stereo binocular microscope, and then the identification was performed using both scanning electron microscope (SEM) and X-ray diffraction (XRD);

Heavy liquid separation: using the bromoform liquid ($CHBr_3$, specific gravity of 2.89) for estimating the heavy mineral content in both the original sample and the fractionated sizes of the scrubbed sample;

The beneficiation processes: were carried out through three stages; the first stage represented in the attrition scrubbing for removal of the clay mineral content as well as the stained oxides, the second was the wet-gravity separation process via Wilfley shaking table No. 13 as a tool for heavy mineral concentration and the third dealt with the high intensity magnetic separator to separate the iron mineral contents and improve the silica sand quality.

3. RESULTS AND DISCUSSION

3.1. UTILIZING THE REMOTE SENSING FOR WHITE SAND EXPLORATION

In this paper, we provide a system for identifying quartz-rich white sand deposits in various geological contexts using thermal ASTER data and silica index (SI) ratio. Ninomiya et al. (2005) used the ASTER thermal bands to create a Quartz Index (QI) for mapping silica-rich units. The silica index (SI) is a band ratio technique that highlights areas with high silica content by using TIR bands 10, 12, and 13 from ASTER data. The Advanced Space borne Thermal Emission and Reflection Radiometer (ASTER) sensor, the ASTER's multi-spectral thermal infrared (TIR) data and the Silica Index ratio (SI) algorithms were successfully used to identify and mapping of quartz rich deposit at local scale over El-Harrah area in northern Bahariya Oasis. The capacity of ASTER thermal infrared images over El-Harrah area in northern Bahariya Oasis of Egypt for accurate and cost-effective identification and mapping of quartz rich deposit at local scale was evaluated. This region's geology comprises a wide range of rock types and unconsolidated surficial materials, many of which are dominated by quartz and carbonate minerals.

The SI is a ratio of two or more TIR bands that are sensitive to quartz and other silicate minerals. Among the previously published silica ratios and indices, two particular silica indices were employed in this work to test the capabilities of various remote sensing technologies in discriminating the silica-rich rock units in El-Harra area and were well validated.

The first SI used is determined by calculating the silica index (SI), which is defined as the ratio of band 13 (10.95–11.65 μm) to band 10 (8.125–8.475 μm), is one way for mapping quartz sand deposits using ASTER TIR data. The SI value is related to the quartz content, hence greater SI values indicate higher quartz content and vice versa. As a result, quartz sand deposits can be distinguished from other silicate rocks by applying a threshold value to the SI image (see Fig. 4) where the bright yellow color indicate the higher content of silica.

The second SI used as the follow:

$$SI = (B10 + B12) / B13,$$

where B10, B12, and B13 are the relative surface emissivity values of ASTER bands 10 (8.125–8.475 μm), 12 (10.25–10.95 μm), and 13 (10.95–11.65 μm).

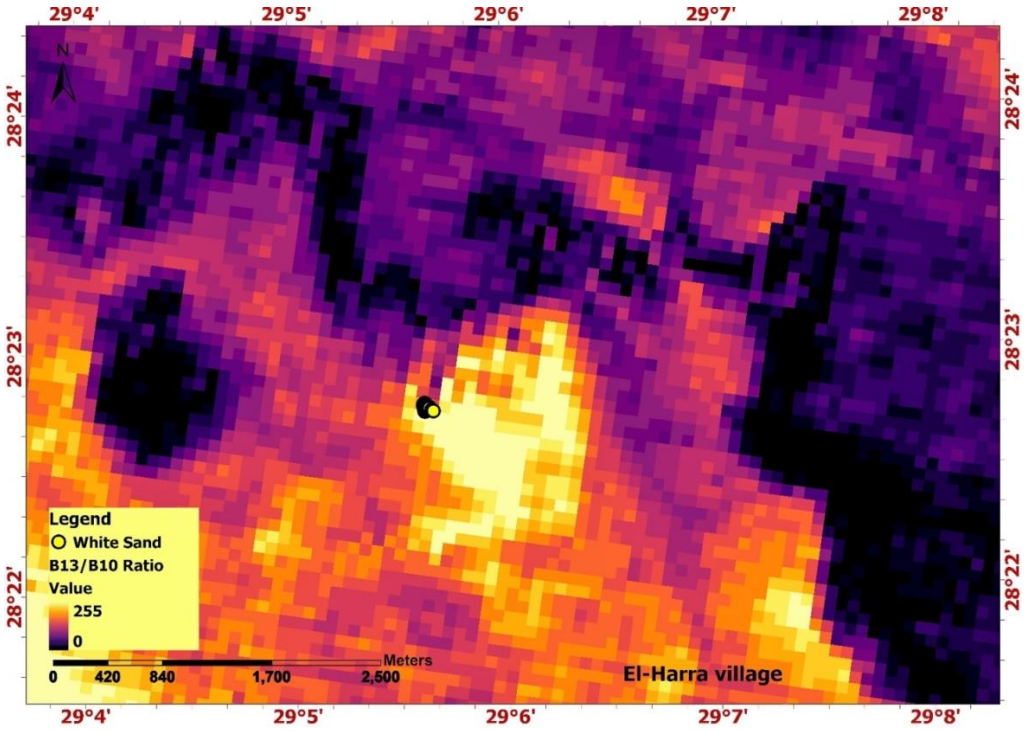

Fig. 4. The first silica index map highlights the quartz rich location identification using the ASTER data at El-Harra area, northern part of Bahariya Depression

The SI range runs from 0 to 2 and converted to digital number DN scale from 0 to 255 for better representation in the final output with higher values signifying more silica. The SI is determined by the shape and position of the quartz reflection feature, which is a significant emissivity peak that occurs between 8 and 9 μm as a result of the Si-O stretching vibration mode. The SI enhances this peak by adding bands 10 and 12, which are placed on both sides of the peak, and dividing by band 13, which is located on the peak's long-wavelength side, where quartz has a low emissivity (see Fig. 5).

In general, the SI value of 1.4 is the preliminary threshold value that distinguishes high-silica areas from low-silica areas, although it could be slightly varied based on the geological environment and the background materials. White sand deposits rich in quartz or other silica-rich units, such as quartzite, chert, and/or silicified rocks, are more likely to be found in areas with SI values above 1.4 while the low-silica elements like carbonate and mafic rocks are likely to be present in regions with SI values below 1.4

(Rockwell and Hofstra 2008).

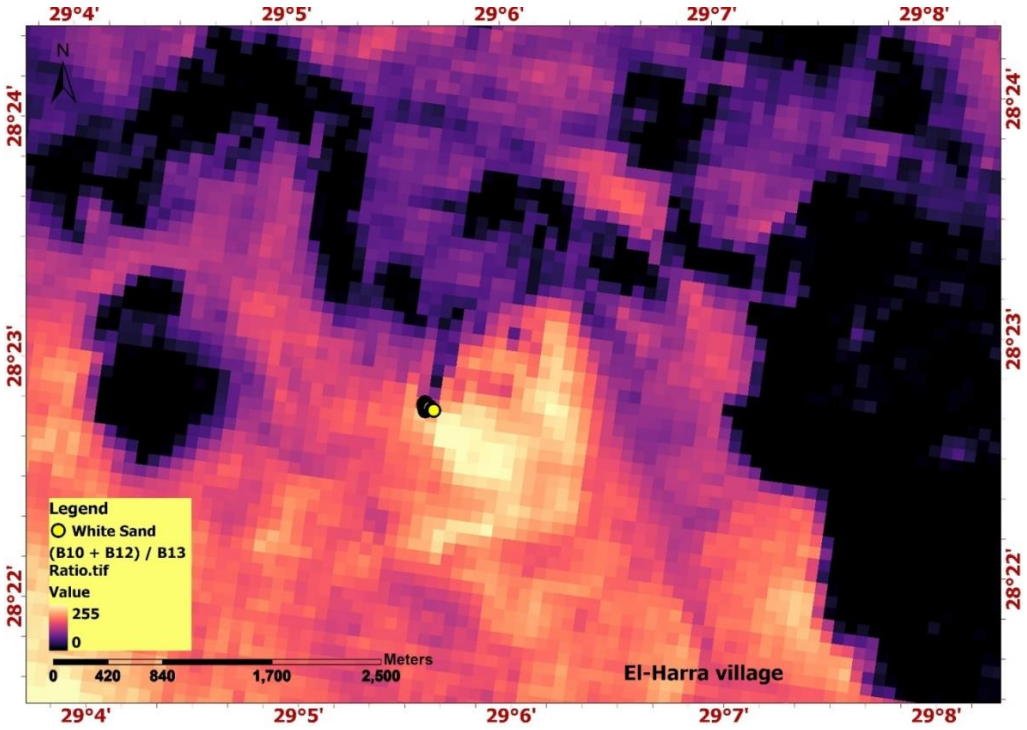

Fig. 5. The second silica index map highlights the quartz rich location identification using the ASTER data at El-Harra area, northern part of Bahariya Depression

Although thermal remote sensing was a valid tool for locating the newly discovered white sand deposit under study, it is important to consider field geological investigation to verify the remote sensing outputs. Verification is necessary to address certain limitations associated with remote sensing techniques, including limited depth penetration (only a few hundred meters can be detected), environmental variables that can make it difficult to identify mineral deposits (such as cloud cover, air moisture, and vegetation cover), interference from non-mineral resources, and difficulty in identifying individual minerals. Therefore, geological field activities were conducted in the El-Harra area and representative samples were collected.

3.2. El-HARRA RAW SAND CHARACTERIZATION

3.2.1. GRAIN SIZE DISTRIBUTION

The mechanical sieving of 300 g from El-Harra white sand for 20 minutes resulted in its fractionation into five grain sizes as (+0.5), (–0.5/+0.25), (–0.25/+0.125), (–0.125/+0.063), and (–0.063 mm), where about 79.5 mass% of the raw sand located in the range of –0.5/+0.125 mm (see Fig. 6), incidentally, is well within the international standard specification for desirable fractions of glassmaking sand. About 10 mass% is above 0.5 mm which has to be discarded as oversize and also 10% mass represented the finer fraction less than 0.125 mm. Subsequently, D10, D30 and D60 corresponding to the size fraction finer than 10%, 30% and 60%, respectively, the uniformity coefficient (CU) and the coefficient of curvature (CC) were determined. Referring to the USCS (ASTM D 2487-93:1994), this sand can be classified as uniformly poorly graded sand (SP) and according to the cumulative curve (see Fig. 7).

Fig. 6. Photographs show different fractions of dry sieving analyses and their corresponding mass percent of the El-Harra raw sand

3.2.2. THE GRAINS MORPHOLOGY

The microscopic observation indicates the presence of different shapes of sand grains

such as; rounded, angular and/or elongated grains. The scanning electron micrographs confirm the optical microscopy observations (see Fig. 8).

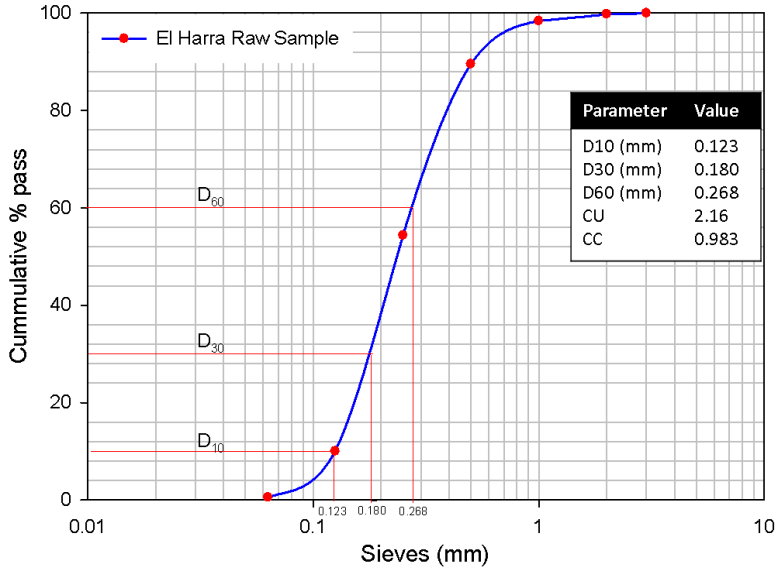

Fig. 7. Particle size distribution of El-Harra raw sand
and its corresponding granulometric parameters

3.2.3. MOISTURE AND FINES CONTENT

The moisture content of El-Harra sand is about 0.21%, in accordance to ISO-15512 this value appears good, on the other hand, the clay content percentage was about 0.9%. Consequently and based on these results, we affirm that El-Harra sand presents less acceptable properties for its future use in carbon-reduction (Boussaa et al. 2018).

3.2.4. CHEMICAL ASSAYS

The chemical composition of both the representative head bulk sample as well as the fractionated samples (after sieving) is shown in Table 1. For the first sight, the percentages of the SiO_2 (96.87%) and the other components in the bulk sample provide an impression that El-Harra white sand is a high grade ore, but referring to the British Standard Specifications (BSS) No. 2975/1988, El-Harra white sand locates close to the fifth grade which is the lowest grade in the BSS and only valid for using in limited traditional applications. On the other hand, the chemical assay for the fractionated sizes revealed that the highest silica content (97.05–98.47% SiO_2) relates to the size range of –0.5/+0.125 mm, but the silica content gradually decreased to about 80% at the size fraction less than 0.063 mm, such decreasing is accompanied by increasing of other components (the lime content (CaO) reaches 9.04%, sulfur (SO_3) reaches 6.63%

SO_3, iron (Fe_2O_3) reaches 0.66% and titania (TiO_2) reaches 1.43%. These results point to that the dry sieving process shows effective upgrading for the white sand purity, where about 80% of the original sand amount has enhanced chemical composition after sieving.

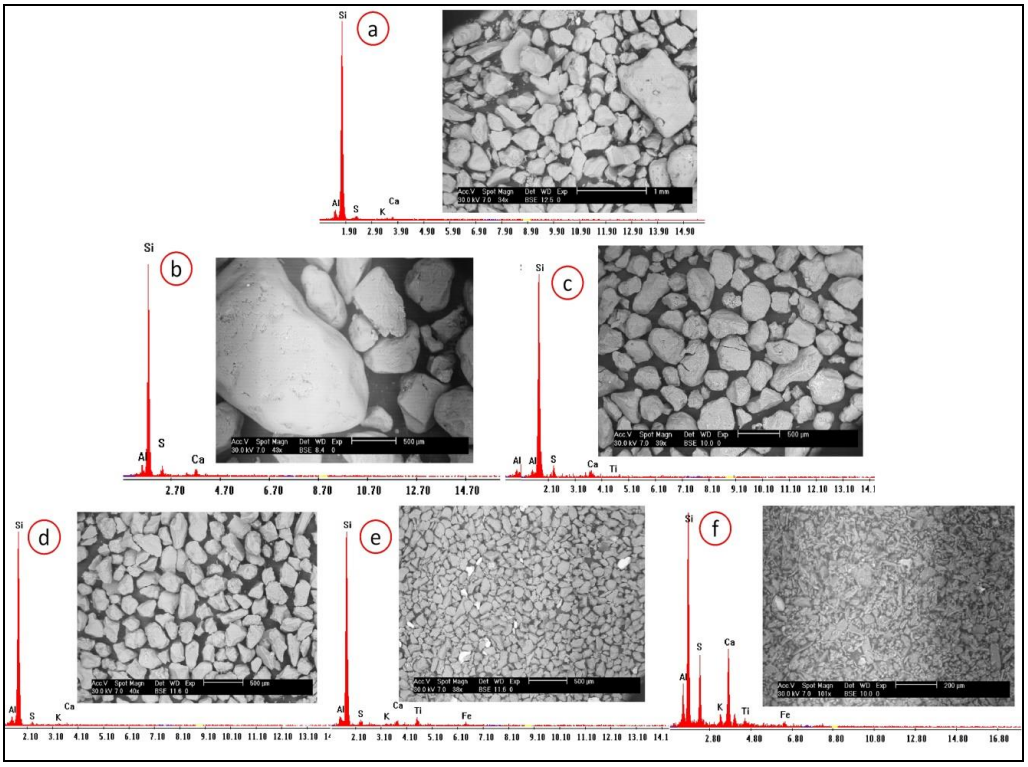

Fig. 8. BSE images and corresponding EDS spectra for El-Harra silica sand sample: a – head sample, b – size fraction (+0.5 mm), c – size fraction (–0.5+0.25 mm), d – size fraction (–0.25+0.125 mm), e – size fraction (–0.125+0.063 mm), f – size fraction (–0.063 mm)

Table 1. XRF elemental oxide analyses for the raw silica sand sample compared with the various size fractions after granulometric analyses

Elemental oxide	Head Sample	Size fractions after dry sieving					
		+1 mm	–1+0.5	–0.5+0.25	–0.25+0.125	–0.125+0.063	–0.063 mm
SiO_2	96.87	95.08	97.02	97.05	98.47	95.11	80.08
Al_2O_3	0.82	0.42	0.46	0.70	0.45	0.84	0.94
CaO	1.27	2.49	2.04	1.45	0.47	1.07	9.04
SO_3	0.19	1.45	0.14	0.25	0.25	0.66	6.63
K_2O	0.15	0.13	0.14	0.15	0.09	0.23	0.95
TiO_2	0.30	0.04	0.06	0.13	0.11	1.47	1.43
Fe_2O_3	0.13	0.08	0.07	0.10	0.07	0.42	0.66

P_2O_5	0.06	0.06	0.07	0.08	0.09	0.13	0.11
Cl	U.D.	U.D.	0.02	0.03	0.02	U.D.	U.D.
MnO	U.D.	U.D.	U.D.	U.D.	U.D.	0.002	U.D.
BaO	U.D.	U.D.	U.D.	U.D.	U.D.	U.D.	0.12
L.O.I	0.21	0.25	0.002	0.08	0	0.08	0.05

3.2.5. MINERALOGICAL CHARACTERIZATION

For El-Harra white sand head sample, the XRD pattern (see Fig. 9) confirms the high crystallinity and the hexagonal crystal system of the quartz grains, where the peaks at 2θ values 26.64°, 20.85°, 50.26° and 60.09° with d-spacing 3.34, 4.25, 1.81, and 1.54 A°, respectively, match the PDF-2 Card No. 85-1054 of quartz mineral and the crystallographic parameters are $a = b = 4.9137$ A° and $c = 5.4051$ A°. In addition to quartz, the peaks of gypsum are also appeared in the XRD pattern.

For the different fractionated sizes, the XRD patterns of sizes (+0.5 mm) and (–0.5/+0.125 mm) revealed that the mineralogical composition is represented in quartz and gypsum as major and minor components respectively (Fig. 10a, b). The kaolin and rutile minerals recorded their attendance, beside the quartz and gypsum, in the fractions of –0.125/+0.063 and –0.063 mm (see Figs. 10c, d). Although they were not detected by the XRD, but both the ilmenite ($FeTiO_3$) and leucoxene minerals were recorded by the SEM technique in the fractions less than 0.125 mm (as will be shown later on). Such mineralogical composition is in full matching with the chemical composition results (Table 2), where the highest values of Al_2O_3, CaO, SO_3, TiO_2 and Fe_2O_3 were recorded in the grain sizes less than 0.125 mm as reflection to presence of considerable amounts of kaolin [$Al_2Si_2O_5(OH)_4$], gypsum ($CaSO_4 \cdot 2H_2O$) as well as rutile, ilmenite and leucoxene minerals in these fractions particularly the size less than 0.063 mm.

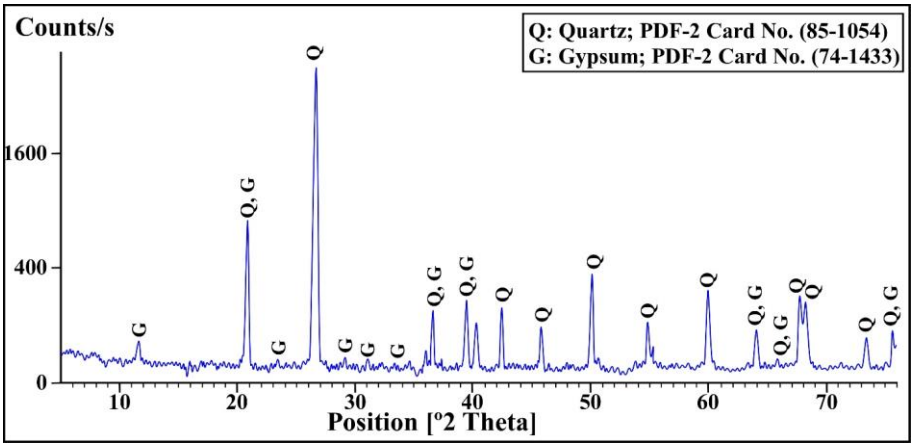

Fig. 9. XRD diffractograms for El-Harra raw sand

On the other hand, the heavy minerals components and quantity were identified after the heavy liquid separation for the head bulk sample as well as the other conducted fractions. The stereo microscopic and SEM investigations pointed to that the heavy minerals are represented by rutile, ilmenite, zircon, leucoxene, green silicates and traces of mica minerals (see Figs. 11 and 12). Estimating the heavy minerals amount in the head and fractionated samples (Fig. 13) indicated that the heavy mineral content in the head bulk sample is about 0.3 mass%, while in the fractionated sizes no heavy minerals were found in the size fractions greater than 0.5 mm but their content was gradually increased as we moved to the finer sizes and reached its highest value (2.7 mass %) in the fraction less than 0.125 mm.

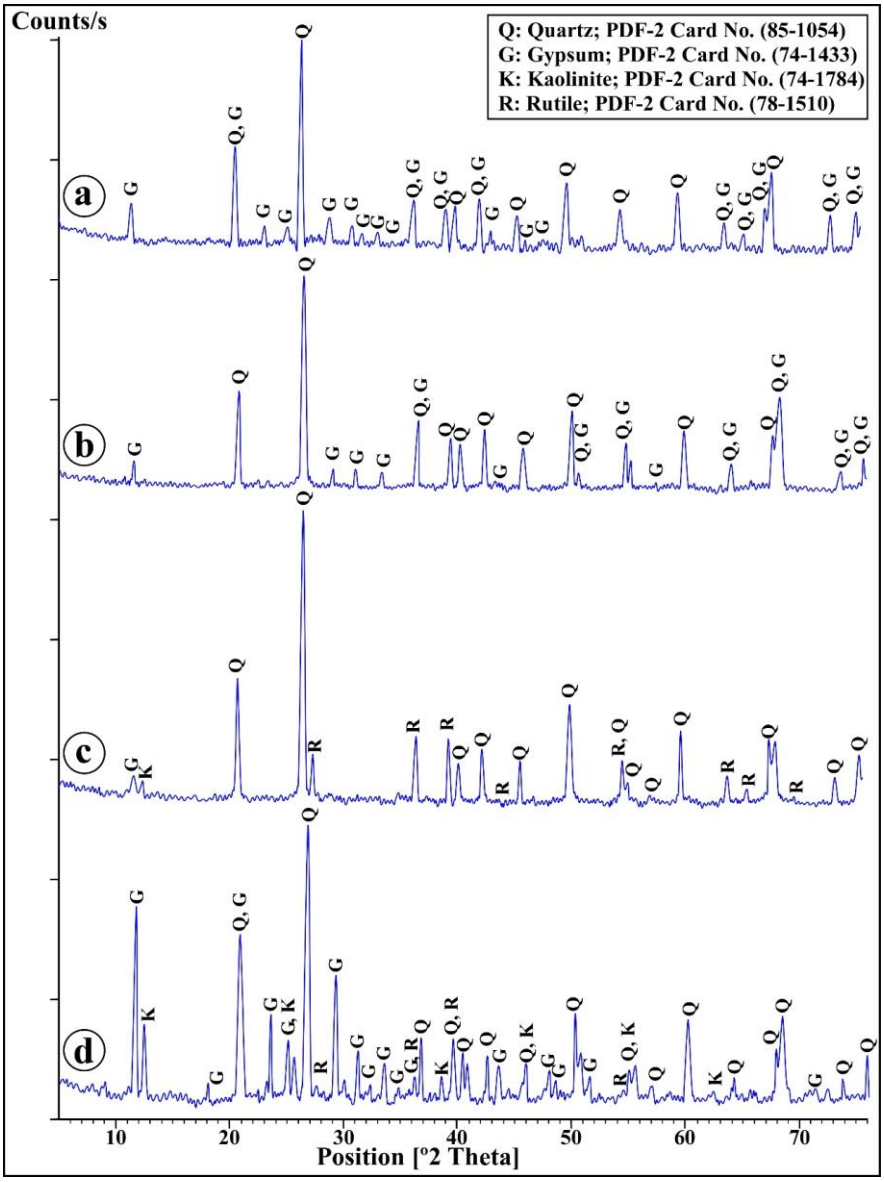

Fig. 10. XRD diffractograms for El -Harra size fractions: (a) size fraction (+0.5 mm), (b) size fraction (–0.5+0.125 mm), (c) size fraction (–0.125+0.063 mm), and (d) size fraction (–0.063 mm)

Table 2. The optimizing operation conditions for the shaking table process

Operation	Roughing	Cleaning
Tested conditions	Optimizing value	Optimizing value
Feed rate	134 g/min	140 g/min
Water flow rate	14 L/min	17.5 L/min
Stroke length	1.5 cm	2 cm
Inclination angle	9°	11°

Generally, the outputs of all the applied investigation and analyses techniques showed that the essential minerals constituents in El-Hara whit sand are as follows: quartz (~95.5 mass %), feldspar (~1.73 mass %), kaolin (~0.9 mass %), gypsum (~0.4 mass %). While the content of the heavy valuable minerals is approximately 0.3 mass %.

3.3. THE BENEFICIATION OF EL-HARRA RAW SAND

The beneficiation process of El-Harra raw sand was conducted using: (1) the attrition scrubbing process, (2) the wet gravity separation technique via shaking table and (3) magnetic separation. Various variables were tested during the processes in order to optimize the operation conditions.

Fig. 11. Stereo microscopic image showing: a – heavy mineral fraction content, b – rutile, c – ilmenite, d – zircon, e – leucoxene, f – green silicates

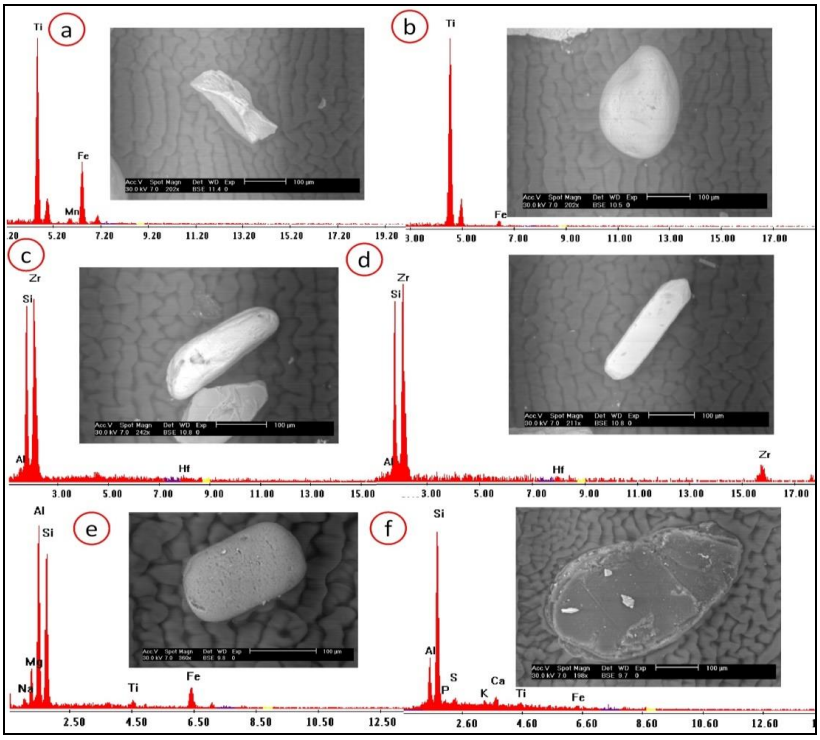

Fig. 12. BSE images and corresponding EDS spectra for heavy minerals: a – ilmenite, b – rutile, c and d – zircon, e – heavy green silicate, f – mica

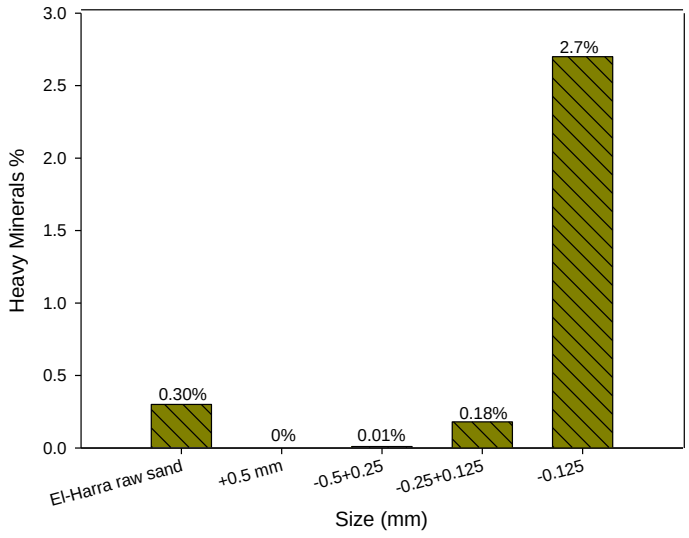

Fig. 13. Heavy mineral assays in El-Harra raw sand in comparison with different size fractions

3.3.1. ATTRITION SCRUBBING

Attrition scrubbing is the simplest technique used for removing the clay-sized particles and metal oxides that adhered to the surfaces of the sand grains by pumping the sand grains together. Firstly, the sample was washed without any stirring, and then the sample was mechanically stirred and washed with distilled water for around 20 minutes at 600 rpm. After complete dryness, the scrubbed sample was weighted and analyzed
using SEM-EDX technique.

The results indicated that about 3.5% of the sample mass was lost after attrition scrubbing process due to reducing some of the kaolin and gypsum content. Also, the scrubbed and dried sample was subjected to grain size analyses and SEM-EDX investigation and the results were compared to their corresponding in the head sample. The total mass percentage of the size fractions (–0.5/+0.25 mm) and (–0.25/+0.125 mm) was enhanced from 79.48% to 82.04% (Fig. 14). It is worth to mention that as the mass % of theses sizes increased as the quality of the white sand increased. Also, the SEM-EDX outputs pointed to enhancing the Si-content and reducing of S, Al, Ca, and K contents after the scrubbing process (Fig. 15), which mean that the chemical characteristics of the studied white sand became more favorable from the add-value point of view. Finally and although the reduction of their content, a faint percentages of S, Al, Ca, and K still present in the scrubbed sample which indicates that the scrubbing process must be repeated to remove them completely.

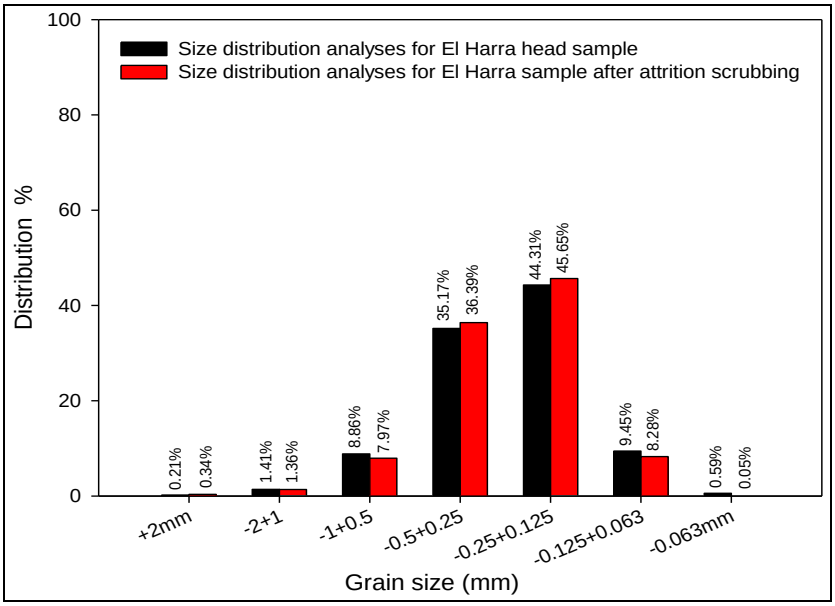

Fig. 14. Grain size distribution analyses for El-Harra raw sand after attrition scrubbing

compared with the original sample

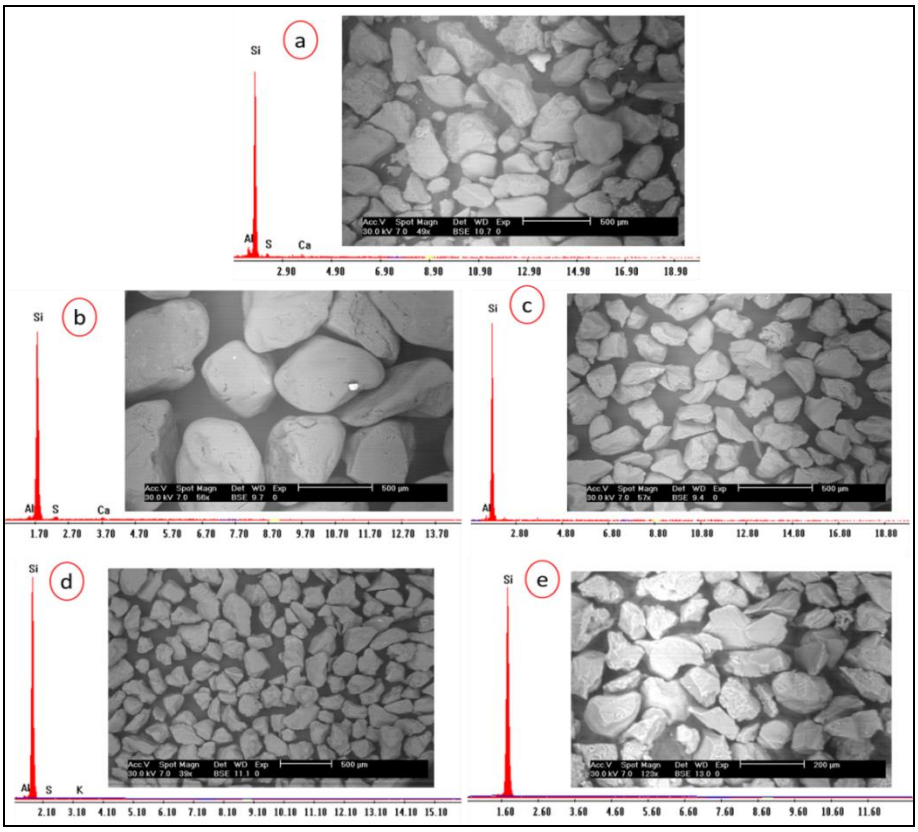

Fig. 15. BSE images and corresponding EDS spectra for El-Harra raw sand after attrition scrubbing: a – head sample, b – size fraction (+0.5 mm), c – size fraction (–0.5+0.25 mm), d – size fraction (–0.25+0.125 mm), e – size fraction (–0.125+0.063 mm)

3.3.2. SHAKING TABLE CONCENTRATION

Shaking table (Model; WILFLEY TABLE NO. 13) was used to improve silica sand grade and concentrate the heavy minerals. To conduct this objective, a rougher concentration stage was initially performed, and then the resulted silica sand product was subjected to cleaning concentration stage to recover the remaining heavy minerals that were not recovered during the initial roughing stage. Some operation conditions were tested and optimized as they are illustrated in Table 2.

The separation processes were carried out on a representative head bulk sample without fractionation as well as three fractions resulted from a fractionated bulk sample into the grain sizes of (–0.5/+0.25 mm), (–0.25/+0.125 mm), and (–0.125 mm). The separation output of the head bulk sample was not successful due to the differen-

tiation in the particle sizes (Fig.16a), while separation for the heavy minerals from the size fraction (–0.5/+0.025 mm) is not visible due to the presence of a very weak percentage of heavy minerals, which does not exceed 0.01% (see Fig. 16b). On the other hand, in the size fraction (–0.25/+0.125 mm) the heavy minerals appear as a fine strip on the table, which have been concentrated and separated from the white sand (Fig. 16c). As for the size fraction (–0.125 mm), the heavy minerals clearly appeared and were separated successfully because this fraction has a high percentage of heavy minerals ~2.7% mass (Fig. 16d), the final products of the separation process for light and heavy fractions were shown in Fig. 17.

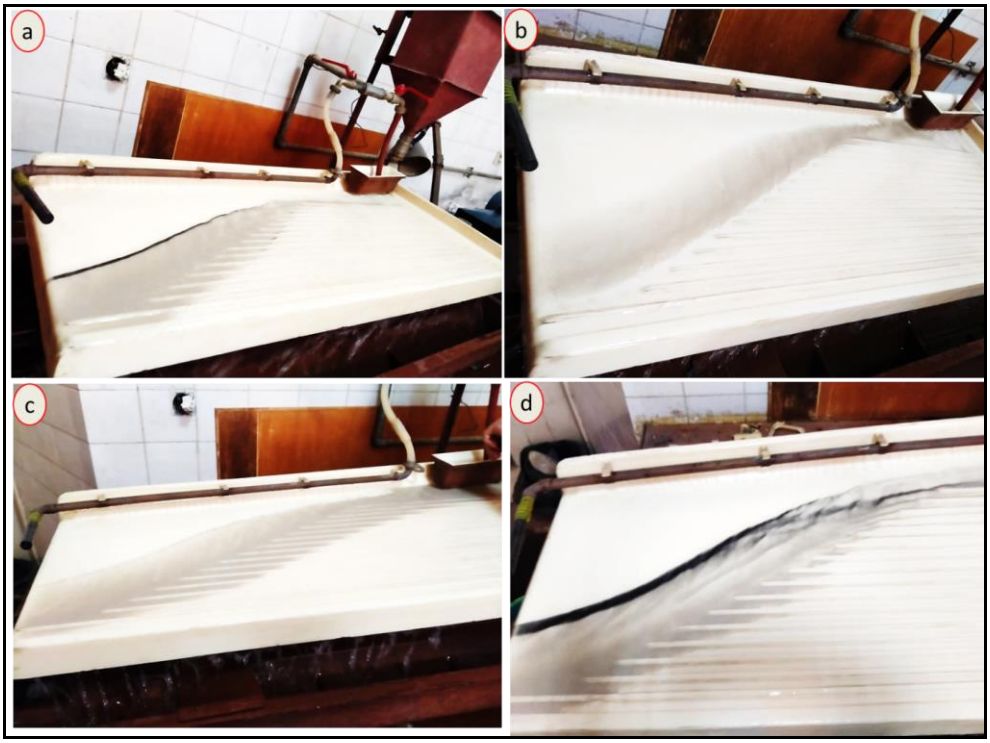

Fig. 16. Photographs showing the gravity separation process via shaking table for El-Harra raw sand compared to the separation of different size fractions: a – head sample, b – size fraction (–0.5+0.25 mm), c – size fraction (–0.25+0.125 mm), d. size fraction (–0.125 mm)

The final products obtained after the rougher and cleaning stages for El-Harra white sand sample were collected, dried, weighed, and chemically analyzed and the results were compared with the head sample and depicted in Table 3. The data of the white sand after the cleaning process confirmed the successful upgrading of El-Harra

white sand where it moves from the fifth grade to the first one according to the British Standard Specifications No. 2975/1988. This means the validity of the beneficiated white sand for utilizing in wide spectrum of advanced and technological industries such as, optics, solar panels optic fibers, LED screens, and hence the beneficiated white sand acquired high add-value.

Elemental oxide	Head sample	Heavy product	Silica sand after rougher stage	Silica sand after cleaning stage
SiO_2	96.87	83.20	98.79	99.53
Al_2O_3	0.82	0.47	0.38	0.05
CaO	1.27	0.24	0.20	0.13
SO_3	0.19	0.15	0.10	U.D.
K_2O	0.15	U.D.	0.16	0.14
TiO_2	0.30	11.7	0.23	0.03
Fe_2O_3	0.13	3.62	0.08	0.05
P_2O_5	0.06	0.29	0.07	0.07
MnO	U.D.	0.15	0.008	0.006
BaO	U.D.	U.D.	U.D.	U.D.
V_2O_5	U.D.	0.57	U.D.	U.D.
Cr_2O_3	U.D.	0.56	U.D.	U.D.
HfO_2	U.D.	0.41	U.D.	U.D.
Nb_2O_5	U.D.	0.03	U.D.	U.D.
L.O.I	0.21	0	0	0

Table 3. XRF elemental oxide analyses for El-Harra raw sand compared with the tabling products after rougher and cleaning stages

Fig. 17. Photograph showing shaking table separation products for El-Harra sand

The XRD investigation of silica sand and heavy mineral concentrate after tabling (Fig. 18a, b) showed the silica sand as full pure product where no other minerals except the quartz were recorded, while for the heavy mineral concentrate, rutile, zircon and ilmenite appeared with a percentage of quartz.

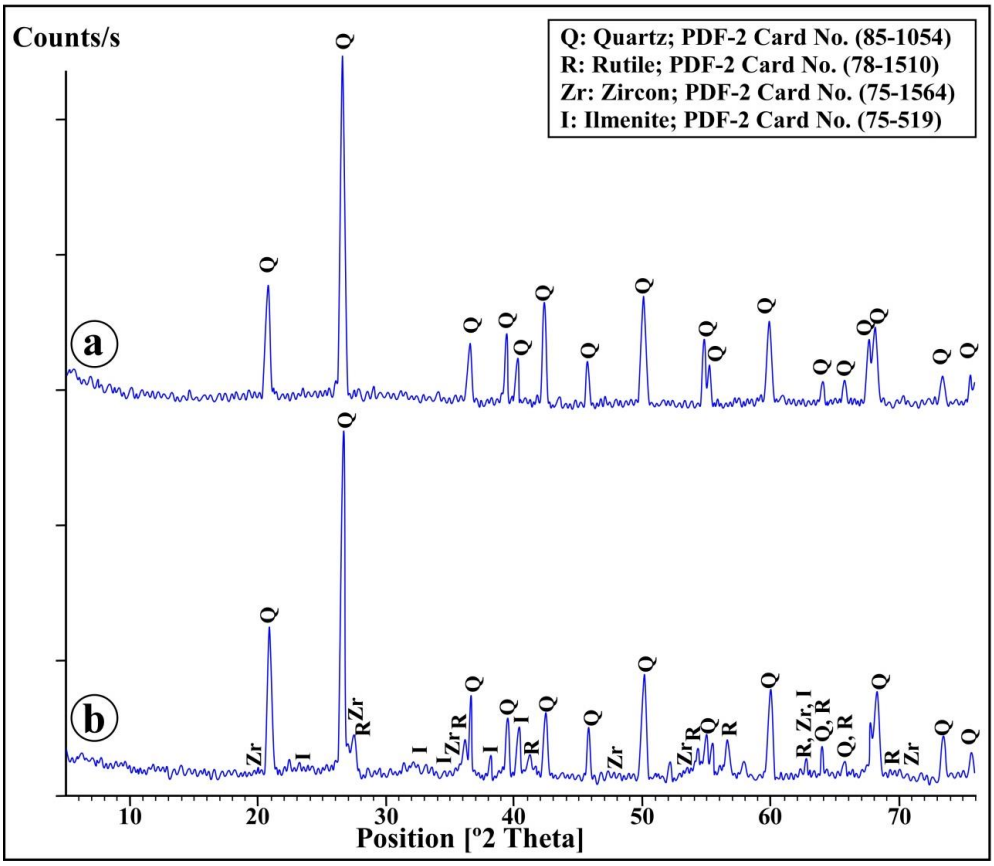

Fig. 18. XRD diffractograms for tabling products for El-Harra raw sand: a – cleaned silica sand, b – heavy mineral concentrate

3.3.3. MAGNETIC SEPARATION

The elemental distribution maps for the heavy mineral concentrate after tabling were shown in Fig. 19 and showed that zirconium, titanium and iron, are distributed and present in acceptable and separable quantities, so it was used as a feed for magnetic separation operations.

Magnetic separation processes via Dry-Carpco high intensity magnetic separator (DHIMS) have been adopted to fractionate and separate the weak para-magnetic minerals from strong para-magnetic from non-magnetic minerals after tabling. The magnetic separation processes were achieved at pre-optimized factors of a medium air gap of 1.5 cm, magnetic field current at 1 and 3 amperes, magnetic roll speed 30 rpm and optimum feed rate 39.2 g/min.

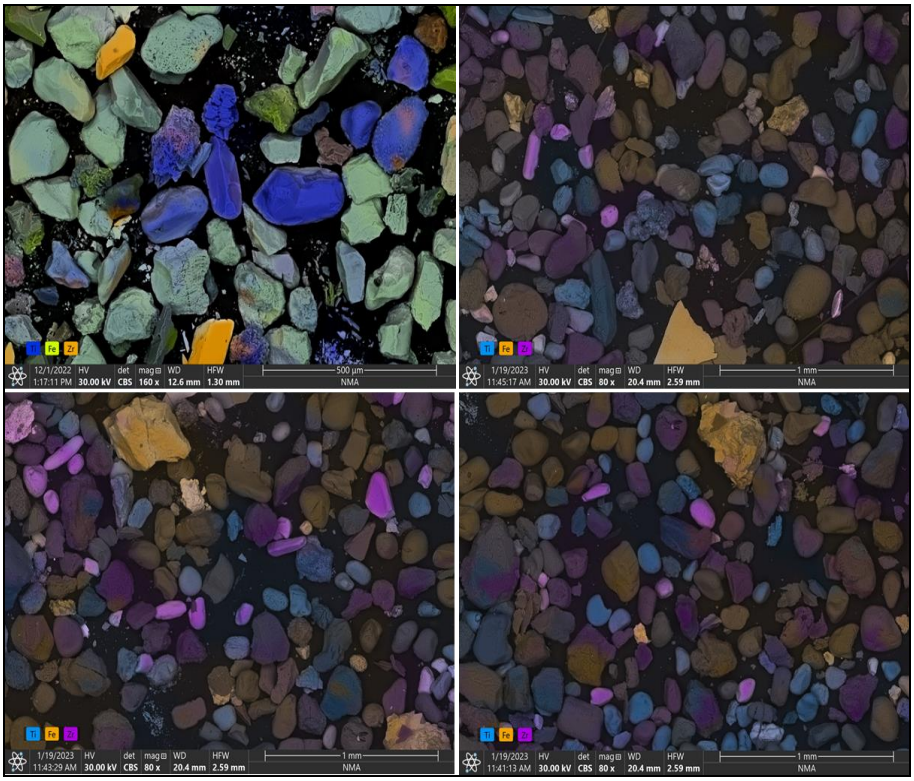

Fig. 19. Elemental distribution maps of the heavy mineral concentrate obtained from the shaking table separation of El-Harra sand

The magnetic separation at 1 and 3 amperes resulted in three magnetic fractions; the first was attained at 1 ampere and contained both ilmenite and leucoxene as paramagnetic minerals, the second and third fractions were conducted at 3 ampere as magnetic portion (include the pyroxenes) and non-magnetic portion which contained both rutile and zircon minerals.

All the applied steps in the beneficiation process of El-Harra white sand were summarized and presented in the proposed flow-sheet in Fig. 20. The physical beneficiation processes succeeded in raising the grade of El-Harra sand from a low-grade to a high-grade that suitable for entering into modern and developed industries. The beneficiation processes also succeeded in concentrating the economic heavy minerals associated with El-Harra sands and separating them as by-products.

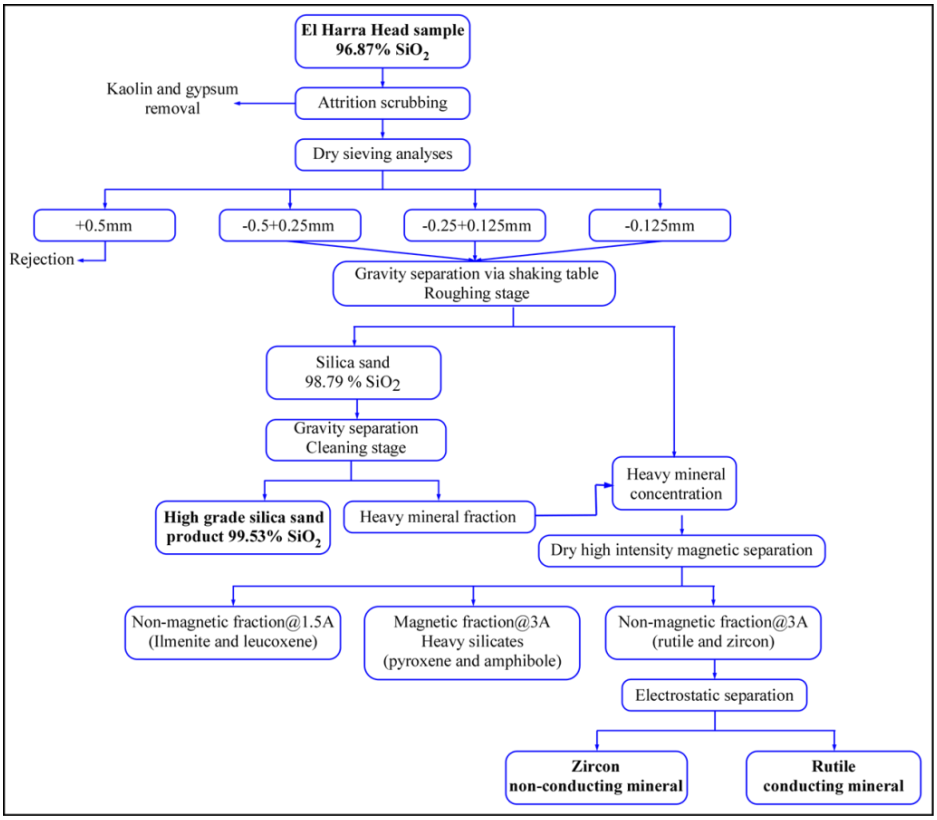

Fig. 20. Proposed flow-sheet for raising the grade of El-Harra raw sand as well as the exploitation of the associated economic heavy minerals

4. SUMMARY AND CONCLUSION

The remote sensing tools appeared as effective and successful method for detection and determination of a new white sand occurrence in El-Harra area which locates to the northern of Bahariya Oasis, Western Desert, Egypt. In the El-Harra region of Egypt's Bahariya Oasis, the SI technique was applied to ASTER data to identify white sand deposits. Our comparison of the results with geological maps and field observations revealed that the SI method was effective in distinguishing quartz-rich white sand deposits from other types of land cover. Moreover, the SI approach enabled the mapping of quartz content fluctuations and spatial distribution within white sand deposits. Our study demonstrates that thermal ASTER data and the SI technique can be utilized to locate and map quartz-rich white sand deposits in arid and semi-arid environments.

The physical, chemical and mineralogical characterization of El-Harra white sand indicated that this sand is not good enough from the purity-grade point of view, where it contains non-desirable grain sizes reached to 20.53 mass %, gangue minerals such as kaolin, gypsum as well as some heavy mineral, these characteristics negatively affected the chemical composition of El-Harra white sand where considerable concentrations of impurities were recorded. Therefore, it was necessary to raise the silica sand grade to acquire add-value and become qualified to use in high-tech applications, as well as getting benefits from its content from the economic heavy minerals.

Consequently, a representative technological sample from El-Hara silica sand was beneficiated through two main techniques; the first was the attrition scrubbing, which proved efficient removing of kaolin and gypsum, and the second was the heavy minerals separation using the wet gravity separation technique via shaking table utilizing two successive stages (roughing and cleaning). The final high grade silica sand product after shaking table contained 99.6% SiO_2, 0.05% Fe_2O_3, 0.03% TiO_2, while Al_2O_3 reached 0.3% that was applicable for the first quality. On the other hand, the magnetic fractionation for the heavy minerals concentrate via DHIMS resulted in separation and concentration of the heavy minerals components into three magnetic portions, where both ilmenite and leucoxene went to the magnetic portion at 1 ampere, the green silicates were concentrated in the magnetic portion at 3 ampere, while both rutile and zircon were confined to the non-magnetic portion at 3 ampere. The last portion has to be subjected for the electrostatic separation to separate rutile and zircon from each other.

By the end of this work, two good benefits are achieved causing add-value for the studied white sand, these benefits represented in:

- Raising the purity-grade of El-Harra white sand to the first grade according to British Standard Specifications for white sands which means higher marketing price and the validity for using in several advanced and respectful industrial applications.
- Good probability for the economical exploitation of the heavy mineral content which found at 0.3 mass % from the original white sand.

ACKNOWLEDGEMENT

The authors gratefully acknowledge the support and assistance provided by our institution (Nuclear Materials Authority).

REFERENCES

ABOUELRESH M.O., EL-NADY H., EL-SHAZLY M., 2007, *Sequence stratigraphy and paleogeographic significance of the Bahariya Formation, El-Harra area, northern Western Desert, Egypt*, Journal of African Earth Sciences, 48 (1), 34–47.

AFIFY A.M., SANZ-MONTERO M.E., CALVO J.P., WANAS H.A., 2015, *Diagenetic origin of iron-stone crusts in the Lower Cenomanian Bahariya Formation, Bahariya Depression, Western Desert, Egypt*, Journal of African Earth Sciences, 101, 333–349.

AHMED A., 2011, *Mineralogy and geochemistry of the barite-bearing deposits in the Alem El-Shellef area, Bahariya Oasis, Egypt*, Arabian Journal of Geosciences, 4 (5–6), 853–860.

ALI H.F., GHONEIM S.M., 2022, *Satellite-based silica mapping as an essential mineral for clean energy transition: Remote sensing mineral exploration as a climate change adaptation approach*, Journal of African Earth Sciences, Vol. 196, p. 104683.

AY N., ARICA E., 2000, *Refining Istanbul's silica sand*, www.Ceramicbulletin.org, August 06.

BHATTACHARYA S., DAS S., 1994, *Beneficiation of Glass Sand – A Review*, Transactions of the Indian Ceramic Society, 53, 2, 25–32, DOI: 10.1080/0371750X.1994.10804626.

BOUSSAA S., KHELOUFI A., ZAOURAR N., 2018, *Sand Dune Characterization for Preparing Metallurgical Grade Silicon*, Open Chem., 16, 1227–1232.

British Standard Institution, 1988, *Specification for sand for making colorless glasses*, BS 2975, UK.

EL AGAMI N.L., ABD EL WAHED A.A., HAROUN Y.E., 2005, *Mineralogy, geochemistry and origin of aluminum phosphate-sulfate minerals in G. El Hefuf, Baharyia Oasis, Western Desert, Egypt*. The 4th International Conference on the Geology of Africa, Vol. 2, 269–292.

EL AKKAD S.E., ISSAWI B., 1963, *Geology and iron ore deposits of Bahariya Oasis*, Geol. Surv. Egypt, 18, 300 p.

EL SHARKAWI M.A., EL FIQUI A., EL ALFY M.A., 2006, *Mineralogy and geochemistry of the Bahariya iron ores, Western Desert, Egypt*, Asian Journal of Earth Sciences, 29 (4), 465–474.

EL-ARABY H.A., EL-METWALLY A.I., ABDEL-RAOUF M.M., 2007, *Reservoir characterization of Middle-Late Cretaceous Bahariya Formation, northern Western Desert, Egypt*, Journal of Petroleum Science and Engineering, 56 (1), 36–52.

EL-ZALAKY M.A., ESMAIL E.M., EL ARAFY R.A., 2018, *Assessment of Band Ratios and Feature-oriented principal component selection (FPCS) Techniques for iron oxides mapping with relation to radioactivity using Landsat 8 at Bahariya Oasis, Egypt*, Researcher, 10 (4).

FARMER A.D., COLLINGS A.F., JAMESON G.J., 2000, *The application of power ultrasound to the surface cleaning of silica and heavy mineral sands*, Ultrasonics Sonochemistry, 7, 243–247.

HAROUN Y.S., RASLAN M.F., 2010, *Occurrence of barite mineralization in Bahariya Depression, Western Desert, Egypt*, Physicochem. Probl. Miner. Process., 41–52.

HASSAN M.A., 2004, *Dinosaur discoveries in the Bahariya Oasis, Western Desert of Egypt*, Münchner Geowissenschaftliche Abhandlungen. Reihe A: Geologie und Paläontologie, 47, 135–149.

IBRAHIM N., SERENO P.C., DAL SASSO C., MAGANUCO S., FABBRI M., MARTILL D.M., ZOUHRI S., 2014, *Semiaquatic adaptations in a giant predatory dinosaur*, Science, 345 (6204), 1613–1616.

MORSY M.A., 1987, *Geology and radioactivity of Late Cretaceous–Tertiary sediments in the Northern Western Desert, Egypt*, PhD Thesis, Fac. Sci., Mansoura Univ., Egypt, 351.

NINOMIYA Y., FU B., CUDAHY T.J., 2005, *Detecting lithology with Advanced Spaceborne Thermal Emission and Reflection Radiometer (ASTER) multispectral thermal infrared "radiance-at-sensor" data*, Remote Sensing of Environment, 99, 127–139.

NICHOLSON K., SHARDLOW M., 2017, *Industrial minerals of the United States*, US Geological Survey.

NIGUSSIE A., DEMISSE T., GETANEH W., 2023, *Industrial properties and uses of silica sand from Blue Nile Basin, Central Ethiopia*, Arab. J. Geosci. 16, 213, http://doi.org/10.1007/s12517-023-11302-7

NORTON F.H., 1957, *Elements of ceramics*, Addision-Wesley Publishing Co., Inc., Reading, Massachusetts.

ODEWALE I.O., AJALA L.O., TSE D.T., 2013, *Characterizaton of Unwana Beach Silica Sand and its Industrial Applications*, IJSID, 3 (1), 93–100.

POPA F., MARINCA T.F., NEAMT U.B.V., GABOR M., CHICINA S.I., 2022, *Structural, Chemical and Magnetic Characterization of Quartz Sand from Cluj Area, Romania for Future Beneficiation in the Glass Industry*, Materials, 15, 9026, https://doi.org/10.3390/ma15249026

ROCKWELL B.W., HOFSTRA A.H., 2008, *Identification of quartz and carbonate minerals across northern Nevada using ASTER thermal infrared emissivity data – Implications for geologic mapping and mineral resource investigations in well-studied and frontier areas*, Geosphere, Vol. 4, No. 1, 218–246.

SAID R., ISSAWI B., 1964, *Geology of the northern plateau, Bahariya Oasis, Egypt*, Ann. Geol. Surv. Egypt, 29, 41.

SALLAM H.M., SEIFFERT E.R., DAHIA I.S., AMER E.S., EL-DAWOUDI I.A., 2018, *New Egyptian sauropod reveals Late Cretaceous dinosaur dispersal between Europe and Africa*, Nature Ecology and Evolution, 2 (3), 445–451.

SALLAM H.M., GORSCAK E., O'CONNOR P.M., EL-DAWOUDI I., EL-SAYED S., SABER S., GINGERICH P.D., 2020, *A new deinonychosaurian track from the Bahariya Formation (Early Cenomanian) of Egypt*, Journal of African Earth Sciences, 166, 103898.

TAXIARCHAOU M., PANIAS D., DOUNI I., PASPALIARIS I., KONTOPOULOS A., 1997, *Removal of iron from silica sand by leaching with oxalic acid*, Hydrometallurgy, 46, pp. 215–227.

WILLS B.A., 2016, *Mineral processing technology*, Pergamon Press, New York.